

# Sensitivity of tracers and a stratospheric aircraft perturbation to two-dimensional model transport variations

Eric L. Fleming,<sup>1</sup> Charles H. Jackman, David B. Considine,<sup>2</sup>  
and Richard S. Stolarski  
NASA Goddard Space Flight Center, Greenbelt, Maryland

**Abstract.** We examine the sensitivity of two-dimensional model simulations of stratospheric tracers to uncertainties in the model transport and explore how such uncertainties impact the simulation of a lower stratospheric perturbation due to high-speed civil transport (HSCT) aircraft emissions. To define the transport uncertainty, we vary the model transport fields so that the resulting tracer simulations roughly bracket the observations. This provides an estimate of the upper and lower limits on realistic transport rates in our two-dimensional (2-D) model. Increasing the advective residual circulation strength or the lower stratospheric vertical diffusion ( $K_{zz}$ ) decreases the mean age and residence time of the HSCT emissions and diminishes the negative response in total column ozone globally. Increasing the stratospheric horizontal diffusion ( $K_{yy}$ ) either globally or in the tropics only has the opposite effect of increasing the age and emission residence time and enhancing the negative total ozone response. Uncertainties in the mechanical eddy forcing derivation affect both  $K_{yy}$  and the residual circulation simultaneously, resulting in some cancellation of effects. This produces a smaller range of uncertainty in the tracer and perturbation simulations than given by uncertainties in the circulation or  $K_{yy}$  components separately. The model simulations in the lower and middle stratosphere are relatively insensitive to the strength of the mesospheric gravity wave effects and the magnitude of the horizontal diffusive transport across the tropopause. The base model transport compares most favorably with tracer data and gives a global and annual mean steady state HSCT perturbation response in total ozone of -0.62%, assuming a  $\text{NO}_x$  emission index of 5 g/kg, 500 airplanes, and a 10% gas-to-particle conversion of the  $\text{SO}_2$  emission. For the range of transport uncertainty examined in this study, the global total ozone perturbation response ranges from -0.34% to -0.74%, with a mainly strong correlation between the total ozone response and mean age.

## 1. Introduction

Over the past decade, two-dimensional (2-D) chemistry and transport models have been used to study the impact of a variety of perturbations on stratospheric ozone. These perturbations include natural changes such as solar cycle variability and volcanic eruptions, as well as man-made influences such as halocarbon increases, space shuttle and rocket launches, and emis-

sions from a potential future fleet of high-speed civil transport (HSCT) aircraft. The development and application of 2-D models to these and other stratospheric problems have been widely documented [e.g., Garcia and Solomon, 1983; Weisenstein et al., 1991; Garcia et al., 1992; Kinnison et al., 1994; Stolarski et al., 1995; Jackman et al., 1996; Weisenstein et al., 1996; Rosenfield et al., 1997; Jackman et al., 1998; World Meteorological Organization (WMO), 1999; Kawa et al., 1999; Intergovernmental Panel on Climate Change (IPCC), 1999].

Recent assessment studies have illustrated a strong dependence of these model calculations on the transport rates used in models, and incomplete or improper representation of atmospheric dynamics remains a major source of model uncertainty [Hall et al., 1999; Park et al., 1999; Kawa et al., 1999; IPCC, 1999; WMO, 1999]. Inaccuracies in model transport rates can have a

<sup>1</sup> Also at Science Systems and Applications, Inc., Lanham, Maryland.

<sup>2</sup> Also at Department of Meteorology, University of Maryland, College Park, Maryland.

Copyright 2001 by the American Geophysical Union.

Paper number 2000JD900732.  
0148-0227/01/2000JD900732\$09.00

variety of sources, including errors in the empirical data sets and assumptions in the algorithms used to derive the transport fields, as well as errors introduced by using dynamics that are climatologically based instead of corresponding to a specific year.

In the case of HSCT emissions, uncertainties in the model transport of exhaust from the source region in the midlatitude lower stratosphere to other parts of the atmosphere can lead to significant variations in the amount of ozone destruction incurred. For example, exhaust transported to the troposphere will have little effect on ozone, whereas exhaust transported to the tropical stratosphere can ascend to higher altitudes and lead to greater ozone loss locally as well as globally. Proper determination of transport rates also has implications for modeling the long-term accumulation of exhaust products throughout the stratosphere.

To better understand the effects of these uncertainties, recent studies have examined the sensitivity of 2-D model transport components on the age of air and tracer simulations. *Bacmeister et al.* [1998] examined in detail the effects of horizontal mixing and the prescribed tropical tropospheric heating on the age of air distribution in an interactive 2-D model. Using a 2-D model with an empirically based (noninteractive) transport, *Li and Waugh* [1999] investigated the general sensitivity of the magnitude and distribution of mean age,  $N_2O$ , and  $Cl_y$  to changes in the model circulation and diffusion fields.

A few studies have specifically examined the role of dynamics in 2-D model simulations of a lower stratospheric perturbation such as HSCT emissions. *Jackman et al.* [1991] studied the dependence of varying the transport on 2-D model simulations of base total column ozone and the ozone perturbation due to HSCT  $NO_x$  injections, along with simulations of inert radioactive tracers carbon 14 ( $^{14}C$ ) and strontium 90 ( $^{90}Sr$ ). Their simulations were strongly sensitive to the model dynamics with weaker transport rates generally resulting in less  $^{14}C$  removed from the stratosphere, longer emission residence times, and greater ozone depletion. *Shia et al.* [1998] examined the effect of adjusting the horizontal mixing ( $K_{yy}$ ) rates in their 2-D model to match tropical-midlatitude exchange timescales inferred from tracer observations. They found that the annually averaged global ozone reductions caused by HSCT emissions were enhanced with increased tropical  $K_{yy}$  in the lower stratosphere.

In a previous paper, we described our upgraded "base" model transport formulation which is derived directly from empirical data sets and compares reasonably well with a variety of tracer observations [*Fleming et al.*, 1999]. In the present paper, we extend this work to examine the sensitivity of inert and chemically active tracers to uncertainties in the model transport components. Quantifying all individual sources of uncertainty in our model dynamical fields is outside the scope of this paper. Instead, we roughly estimate the range of transport uncertainty by varying the base trans-

port parameters so that the tracer simulations maintain some agreement with a variety of measurements, including  $CH_4$ ,  $^{14}C$ ,  $N_2O$ , and age of air from  $SF_6$  and  $CO_2$ . We examine the sensitivity to changing the residual circulation throughout the atmosphere; the horizontal diffusion in the stratosphere; the vertical diffusion in the upper troposphere and lower stratosphere; and the gravity wave-induced drag and vertical diffusion in the upper stratosphere and mesosphere. We then apply these transport scenarios to the model simulations of an HSCT perturbation. This allows us to determine a range of uncertainty due to transport in the model computed HSCT perturbation response in total ozone. We will also compare the results from our latest model with those obtained from a previous version of our model transport used in the 1995 NASA assessment [*Stolarski et al.*, 1995].

## 2. GSFC-2D Model Description and Simulations

The 2-D model at NASA Goddard Space Flight Center (GSFC) was originally described by *Douglass et al.* [1989] and *Jackman et al.* [1990]. Recent improvements to the model have been discussed by *Jackman et al.* [1996], and upgrades to the transport formulation are described by *Fleming et al.* [1999]. We have updated the gas phase reaction rates and photolysis cross sections to the Jet Propulsion Laboratory (JPL) 2000 recommendations [*Sander et al.*, 2000].

For the transport experiments discussed in this paper, we will show model simulations of several long-lived tracers, including  $CH_4$ ,  $N_2O$ ,  $^{14}C$ , and mean age of air derived from  $SF_6$  and  $CO_2$ , along with simulations of an HSCT perturbation. We note that in this study, we take the age of air to be relative to the model tropical tropopause (equator, 100 mbar) as opposed to the global mean surface value used previously [*Fleming et al.*, 1999].

For the  $N_2O$  simulations we use time-dependent boundary conditions from *WMO* [1999]. For  $CO_2$  we use time-dependent boundary conditions based on monthly mean global surface observations for 1979 to 1995 [*Conway et al.*, 1994], with these values extended through 1997 by increasing the 1995 values by 1.4 ppmv/yr. The small  $CO_2$  source from  $CH_4$  oxidation is included, with time-dependent  $CH_4$  surface boundary conditions used from *WMO* [1999]. For the  $^{14}C$  simulation, initial conditions are taken from *Prather and Remsberg* [1993], with the latitude and altitude dependent distributions specified on October 15, 1963. Time and hemisphere dependent ground boundary conditions for  $^{14}C$  were also specified from *Prather and Remsberg* [1993].

For the HSCT perturbation simulations the model was run for 20 years to obtain a seasonally repeating steady state solution, with all results shown from the final year of the calculation. All simulations are made for

2015 conditions of aircraft emissions and surface boundary conditions for the background atmosphere [Kawa *et al.*, 1999; IPCC, 1999]. These boundary conditions correspond to a total  $\text{Cl}_y$  loading of 3.0 ppbv and a total  $\text{Br}_y$  loading of 12.5 pptv. Throughout the paper we compare the perturbation simulation, which includes both supersonics and subsonics, with the reference simulation, which includes subsonic aircraft only. For the simulations of supersonic aircraft we assume a  $\text{NO}_x$  emission index (EI) of 5 g/kg, 500 airplanes, and a 10% gas-to-particle conversion of the  $\text{SO}_2$  emission. These runs correspond to the NASA Atmospheric Effects of Supersonic Aviation (AESA) assessment scenarios 1 and 9 [Kawa *et al.*, 1999] and the Intergovernmental Panel on Climate Change (IPCC) scenarios D and S1k [IPCC, 1999].

### 3. Results

In this section, we examine the sensitivity of the tracer and HSCT simulations to uncertainties in the model transport components. Uncertainty in our model dynamical fields can arise from several sources, such as the measurement, algorithmic, and numerical uncertainties in the original meteorological analyses and heating rate calculations, with the latter having a source of uncertainty in the temperature and constituent fields used; and, uncertainties in the eddy diffusion parameterizations which utilize higher order derivatives of the meteorological analyses. There is also uncertainty due to small-scale, seasonal, and/or interannual geophysical variability not resolved in the original meteorological data or in the derived model transport fields. Rigorously quantifying all such uncertainties is outside the scope of this study. Instead, we use the available tracer observations as an approximate guide to illustrate the degree to which the model transport can be changed and

still be reasonably realistic. Although there is some uncertainty in the tracer data due to, for example, incomplete resolution of seasonal and interannual variability [e.g., Hall *et al.*, 1999], we use the available observational coverage to roughly constrain the lower and upper limits of realistic transport rates in the model.

#### 3.1. Residual Circulation

Our model residual circulation is driven by a combination of net diabatic heating, sensible and latent heat release in the troposphere, and mechanical forcing from eddy motions. While net radiative heating calculations in zonal mean models are regarded as fairly accurate, determination of mechanical wave drag and sensible and latent heating is a major source of uncertainty. In this section we examine the uncertainty in the strength of the residual horizontal and vertical velocities (residual circulation) throughout the troposphere, stratosphere and mesosphere due to the combination of these heating and wave drag processes (the horizontal and vertical diffusion parameters remain unchanged). In section 3.5 we consider the effects of self-consistent changes to the circulation and horizontal diffusion fields.

**3.1.1. Diagnostic tracers.** Figure 1 shows latitudinal profiles of the annual mean age of air ( $\Gamma$ ) (relative to the tropical tropopause) derived from  $\text{SF}_6$  for the base model (scenario A in Table 1), along with two transport scenarios in which the circulation strength has been decreased (scenario B, dashed line) and increased (scenario C, dash-dotted line) by 25% from the baseline case.

Also shown in Figure 1 are  $\Gamma$  derived from in situ ER-2 aircraft measurements of  $\text{SF}_6$  (triangles) and  $\text{CO}_2$  (plus signs) compiled from several field campaigns during 1992 to 1997 [Elkins *et al.*, 1996; Boering *et al.*, 1996]. As discussed in previous work, the stratospheric  $\Gamma$  inferred from observations of  $\text{SF}_6$  and annually aver-

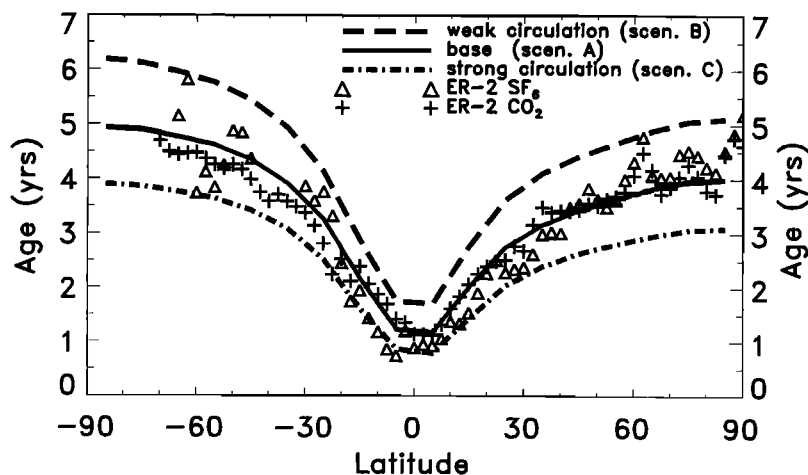


**Figure 1.** Age of air derived from model simulations of  $\text{SF}_6$  at 20 km for the base scenario A (solid line), the weak circulation scenario B (dashed line), and the strong circulation scenario C (dash-dot line). Also shown are age of air determined from ER-2 measurements of  $\text{SF}_6$  (triangles) and  $\text{CO}_2$  (pluses). Ages are taken relative to the tropical tropopause. See text for details.

**Table 1.** Globally Averaged Mean Age (Relative to the Tropical Tropopause) and the HSCT Total Ozone Perturbation Response for Each Transport Scenario (All Values Are Annual Averages)

Scenario	Description	Mean Age, Years			Total Ozone Change, %		
		19 km	27 km	35 km	Global	NH	SH
A	base (1999 model transport)	2.7	4.0	4.6	-62	-62	-62
B	weak circulation (base decreased by 25%)	3.4	5.5	6.3	-71	-73	-68
C	strong circulation (base increased by 25%)	2.1	2.9	3.3	-53	-53	-53
D	small lower stratospheric $K_{zz}$ ( $0.001 \text{ m}^2/\text{s}$ )	3.1	4.3	4.9	-68	-65	-71
E	large lower stratospheric $K_{zz}$ ( $0.2 \text{ m}^2/\text{s}$ )	1.8	3.0	3.6	-34	-41	-26
F	weak mesospheric gravity wave drag, $K_{zz}$	2.8	4.1	4.8	-61	-61	-62
G	strong mesospheric gravity wave drag, $K_{zz}$	2.5	3.7	4.2	-60	-64	-56
H	$K_{yy}/2$ (above tropopause)	2.3	3.0	3.3	-53	-62	-41
I	$K_{yy}^*2$ (above tropopause)	3.3	5.7	6.7	-74	-65	-83
J	$K_{yy}/2$ + wave drive/2 (above tropopause)	3.0	3.9	4.2	-62	-73	-51
K	$K_{yy}^*2$ + wave drive*2 (above tropopause)	2.0	3.6	4.2	-53	-49	-58
L	large cross-tropopause $K_{yy}$	2.8	4.1	4.7	-62	-63	-61
M	small tropical stratospheric $K_{yy}$ ( $0.01 \times 10^6 \text{ m}^2/\text{s}$ )	2.7	3.4	3.5	-53	-59	-46
N	large tropical stratospheric $K_{yy}$ ( $0.2 \times 10^6 \text{ m}^2/\text{s}$ )	2.7	4.4	5.1	-68	-62	-74
O	1995 model transport	1.1	2.2	2.8	-25	-29	-20
P	combination, long residence time	4.2	6.4	7.3	-81	-73	-90
Q	combination, short residence time	1.8	2.7	3.1	-42	-50	-32

aged  $\text{CO}_2$  show good agreement [e.g., *Hall et al.*, 1999; *Park et al.*, 1999]. Consistent with the observations shown by *Hall et al.* [1999], the data in Figure 1 are averaged over  $2.5^\circ$  latitude bins, for 19.5–21.5 km for  $\text{CO}_2$  and 19–21 km for  $\text{SF}_6$ . Following *Boering et al.* [1996], mean age derived from  $\text{CO}_2$  is computed with respect to the observed  $\text{CO}_2$  time series at the tropical tropopause [*Andrews et al.*, 1999], accounting for the small  $\text{CO}_2$  source from  $\text{CH}_4$  oxidation. Mean age from  $\text{SF}_6$  is computed following *Volk et al.* [1997], which uses the global mean surface time series compiled by *Geller et al.* [1997] as the reference function. To be consistent with the  $\text{CO}_2$  ages (and the model ages), we have subtracted 0.8 years from the observed  $\text{SF}_6$  ages to approximate the time lag from the global mean surface to the tropical tropopause [*Volk et al.*, 1997].

Figure 2 shows vertical age profiles from the three model circulation scenarios and balloon observations at low, middle, and high latitudes. These data have been averaged in 1-km bins and include in situ  $\text{CO}_2$  and  $\text{SF}_6$  measurements taken as part of the Observations of the Middle Stratosphere (OMS) campaign [*Hall et al.*, 1999; A. E. Andrews et al. (“Mean ages of stratospheric air derived from in situ observations of  $\text{CO}_2$ ,  $\text{CH}_4$ , and  $\text{N}_2\text{O}$ ”, submitted to *Jour. of Geophys. Res.*, 2001); F. L. Moore et al., manuscript in prepara-

tion, 2001], along with laboratory measurements of  $\text{SF}_6$  collected by a balloon-borne cryogenic whole-air sampler (CWAS) flown at middle and high latitudes [*Harnisch et al.*, 1996]. The low-latitude data in Figure 2a are averages over several OMS balloon flights at  $7^\circ\text{S}$  during February and November 1997. The midlatitude data in Figure 2b include  $\text{CO}_2$  and  $\text{SF}_6$  ages from one OMS flight during September 1996 at  $35^\circ\text{N}$ , along with  $\text{SF}_6$  ages from whole-air samples taken during one September 1993 flight at  $44^\circ\text{N}$ . The high-latitude data in Figure 2c include  $\text{CO}_2$  and  $\text{SF}_6$  ages from one OMS flight during June 1997 at  $65^\circ\text{N}$ , along with  $\text{SF}_6$  ages from whole-air samples taken at  $68^\circ\text{N}$  averaged over three flights inside the polar vortex during January–March 1992 (squares), and one flight outside the vortex during March 1995 (asterisks). These mean ages have been computed as in Figure 1.

Figures 1 and 2 show the general increase in age with decreasing model circulation strength which is also seen in the globally averaged  $\Gamma$  at different stratospheric altitudes listed in Table 1. The age differences between the different circulations are largest in the middle stratosphere at middle and high latitudes. We also note that the vertical gradients and the latitudinal gradients between the tropics and midlatitudes decrease with increasing circulation strength, illustrating that such gra-

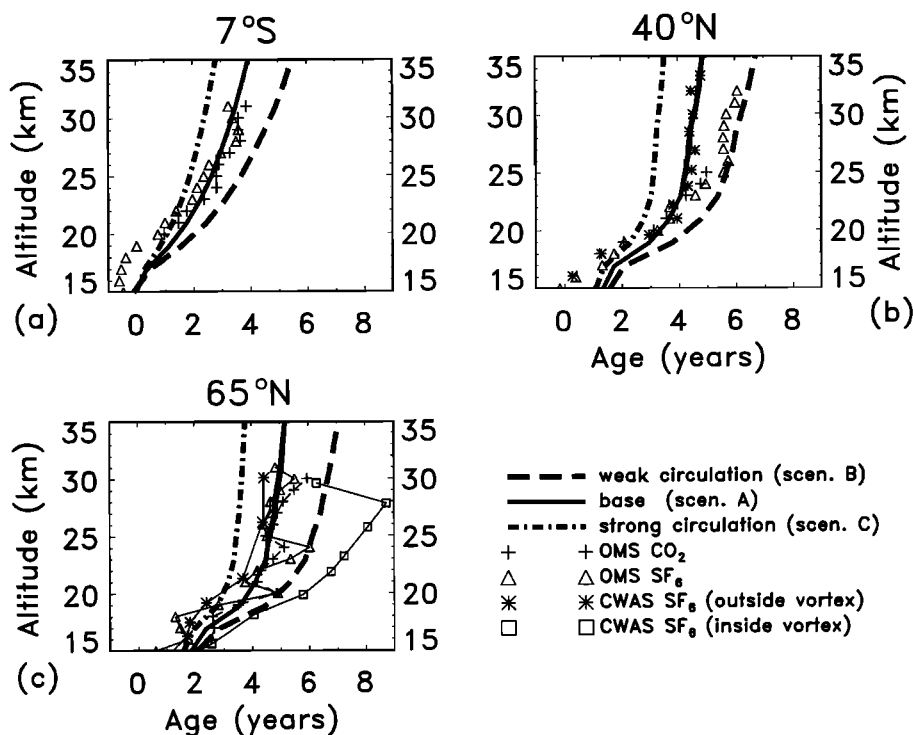


**Figure 2.** Vertical profiles of age of air derived from model simulations of SF<sub>6</sub> for the base scenario A (solid line), the weak circulation scenario B (dashed line), and the strong circulation scenario C (dash-dot line). Also shown are age of air determined from balloon measurements of SF<sub>6</sub> and CO<sub>2</sub> as discussed in the text. Ages are taken relative to the tropical tropopause.

dients can be modified by the residual circulation as well as the horizontal or vertical diffusion rates. This latter result is consistent with the analytical modeling study of *Neu and Plumb* [1999].

Figures 1 and 2 show that while the baseline transport (scenario A) provides the best overall agreement with the data, both the weak and strong circulations are within reasonable agreement with the observations in some of the comparisons. For example, at 20 km in the tropics, the base and strong circulations compare well with the data, whereas the weak circulation produces ages that are a bit too old. However, at midlatitudes (Figure 2b) the weak circulation compares best with the OMS data (triangles) above 20 km, while the base model agrees best with the data of *Harnisch et al.* [1996] (asterisks). Note that these two midlatitude data sources show age differences of  $\sim 1$  year in the middle stratosphere, even though they are for similar latitudes and seasons (September). Some of this difference may be due to interannual dynamical variability since the data were taken during different years (1996 versus 1993).

There is a relatively large spread in the winter data at high latitudes in Figure 2c, due to age differences between air inside (squares) and outside (asterisks) the polar vortex. The single OMS balloon flight during June 1997 (pluses and triangles) shows ages which are mostly similar to extra-vortex air, however, there are shallow

layers of older air at 20 and 24 km in this profile which likely reflect remnants of the winter vortex [*Ray et al.*, 1999]. All three model circulations are generally close to the range of these data. However, even the slow circulation gives ages that are significantly younger than the inner vortex data profile (squares) at 22–28 km. While this may indicate deficiencies of a zonal mean model in simulating the northern polar vortex region which can exhibit substantial longitudinal variability, it could also be indicative of a mesospheric photochemical loss incurred by SF<sub>6</sub> which would bias the inferred mean age to be older than the actual age [*Hall and Waugh*, 1998].

To further examine the high latitude model-data comparisons, Figure 3 shows vertical profiles of CO<sub>2</sub> plotted against N<sub>2</sub>O at polar latitudes in each hemisphere. These observations are taken from ER-2 flights for the time periods and latitude ranges indicated in Figure 3 and are averaged over 1 ppbv N<sub>2</sub>O bins. N<sub>2</sub>O and CO<sub>2</sub> generally exhibit a compact relationship in the lower stratosphere [*Boering et al.*, 1996; *Strahan et al.*, 1998], except where mixing of midlatitude and vortex air creates “mixing lines” in the N<sub>2</sub>O–CO<sub>2</sub> correlation [*Waugh et al.*, 1997]. Figure 3 is also representative of the mean age on N<sub>2</sub>O surfaces, which have a reasonably constant relationship outside of the tropics where the CO<sub>2</sub> seasonal cycle has damped out [*Park et al.*, 1999; *Andrews et al.*, 2000]. To avoid minor errors in the age derivation caused by the CO<sub>2</sub> annual cycle and/or incom-

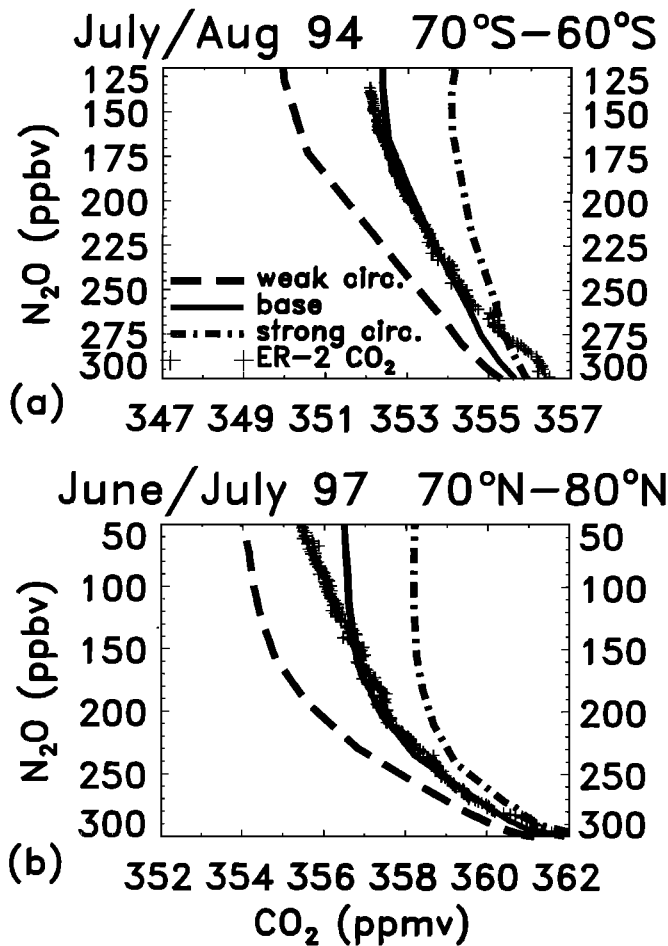


**Figure 3.** Vertical profiles of  $\text{CO}_2$  (ppmv) versus  $\text{N}_2\text{O}$  (ppbv) from ER-2 measurements (pluses) and time-dependent model simulations from the base scenario A (solid line), the weak circulation scenario B (dashed line), and the strong circulation scenario C (dash-dot line) for the latitudes and months/years indicated.

plete resolution of the  $\text{CO}_2$  time history at the tropical tropopause, we show just the  $\text{CO}_2$  concentration, rather than mean age, plotted against  $\text{N}_2\text{O}$  in Figure 3.

The base model simulation is generally quite close to the data in both Figures 3a and 3b. The  $\text{CO}_2$ – $\text{N}_2\text{O}$  correlation is strongly sensitive to the circulation so that for a given value of  $\text{N}_2\text{O}$ , the  $\text{CO}_2$  concentrations increase and the mean age decreases with increasing circulation strength, with this sensitivity increasing with height. At the lowest  $\text{N}_2\text{O}$  values of 125 ppbv at high southern latitudes during winter (Figure 3a), the weak and strong circulations show a  $\text{CO}_2$  difference of 4.5 ppmv, which corresponds to an age difference of  $\sim 3$ – $3.2$  years (assuming a linear  $\text{CO}_2$  increase of 1.4–1.5 ppmv/yr at the ground). This is consistent with the model  $\Gamma$  results derived from  $\text{SF}_6$  at high latitudes in Figure 2c. However, the southern vortex  $\text{CO}_2$  –  $\text{N}_2\text{O}$  observations in Figure 3a indicate ages that are close to the base model and significantly younger than the weak circulation case, at least at heights above  $\text{N}_2\text{O}$  levels of 275 ppbv up to the highest ER-2 altitudes (21 km).

This is in contrast with the  $\text{SF}_6$ -observed age profile in the Northern Hemisphere (NH) inner vortex in Figure 2c, which indicates significantly older air than simulated by the model weak circulation.

We note that the tracer sensitivity to the model circulation strength and comparisons with data shown in Figure 3 are typical of most latitudes and seasons. An exception is at the lowest levels of the Southern Hemisphere (SH) profile in Figure 3a, in which all three circulations show significant differences with the data. This could be due to incomplete resolution of processes near the tropopause in the model and/or localized effects in the data.

As an additional transport diagnostic, we compare the model time-dependent simulations of the inert radioactive tracer, carbon 14, with observations from Kinnison *et al.* [1994]. Carbon 14 has a chemical lifetime and lower stratospheric source region similar to long-lived products of supersonic aircraft exhaust. Therefore model-measurement comparisons of  $^{14}\text{C}$  are especially helpful in evaluating the accuracy of model transport and model assessments of the effects of stratospheric aircraft [e.g., Jackman *et al.*, 1991; Prather and Remsberg, 1993; Kinnison *et al.*, 1994].

Figure 4 shows  $^{14}\text{C}$  observations along with model simulations from the different circulation scenarios at  $31^\circ\text{N}$  for July 1966, 2 years and 9 months after initialization. There are only small differences among the model scenarios below  $\sim 18$  km, with more significant differences above 18 km. All three scenarios reproduce the strong vertical gradient up to 20 km, with a sharp transition to the weak gradient above 20 km seen in

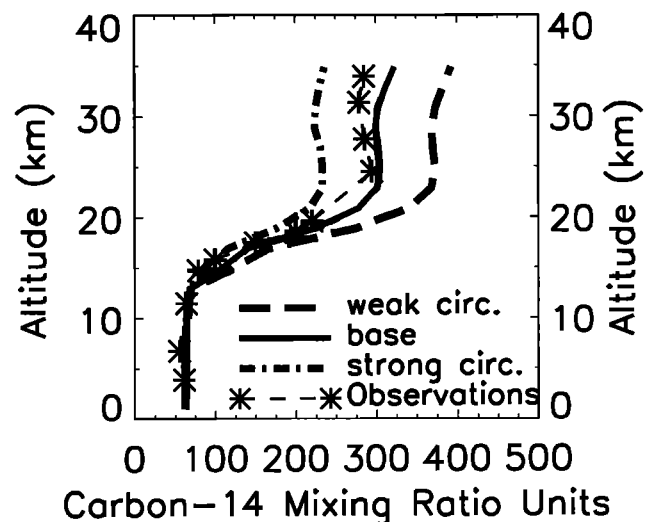


**Figure 4.** Vertical profiles of carbon 14 at  $31^\circ\text{N}$  for July 1966 from time-dependent model simulations from the base scenario A (solid line), the weak circulation scenario B (dashed line), and the strong circulation scenario C (dash-dot line), along with observations (Kinnison *et al.* [1994], dashed-asterisk). Values are in mixing ratio units, defined as  $10^5$  atoms of  $^{14}\text{C}$  per gram of dry air.

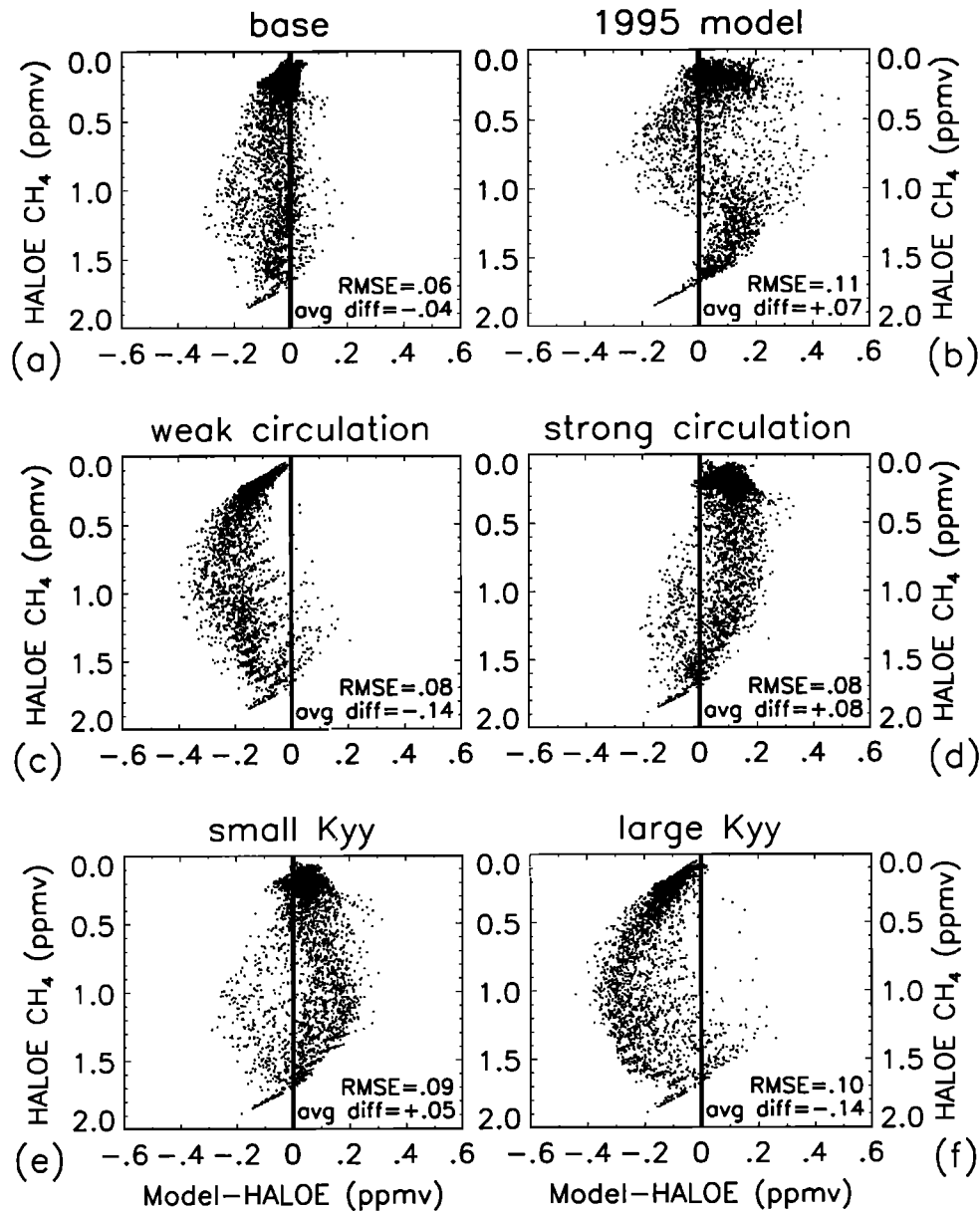


**Figure 5.** Scatterplots of the model minus HALOE difference in CH<sub>4</sub> (ppmv) versus HALOE CH<sub>4</sub> (ppmv) for the base scenario A, the 1995 model transport scenario O, the circulation scenarios B and C, and the  $K_{yy}$  scenarios H and I. Each point represents a monthly mean value of the model and climatological zonal mean HALOE data averaged over 1994-1999, and binned at every 10° latitude for 80°S-80°N and 100-0.1 mbar at the standard UARS pressure levels. To correspond to the HALOE time period, the model values have been scaled to the 1994 CH<sub>4</sub> boundary condition [WMO, 1999]. The average difference (model-HALOE) and the root mean square error (RMSE) of the model compared to HALOE after removing the average difference, are also indicated for each scenario.

the observations. This transition becomes increasingly more acute with decreasing circulation strength. Note that the model circulation dependence of the overall vertical structure of <sup>14</sup>C is very similar to the mean age simulations in Figure 2b. However, the comparison in Figure 4 reveals that the base or strong circulation gives the best agreement with the <sup>14</sup>C data, whereas the base or weak circulation gave the best agreement with the midlatitude data profile of  $\Gamma$  in Figure 2b.

As a final transport diagnostic, we compare model simulations of the long-lived, chemically active tracer CH<sub>4</sub> with data from the Halogen Occultation Experiment (HALOE) on the Upper Atmospheric Research Satellite (UARS). Figure 5 shows scatterplots of the difference between steady state model simulations and climatological monthly mean HALOE (version 19) CH<sub>4</sub>, plotted against the HALOE data for several transport scenarios. The HALOE data are 6 year means (1994-

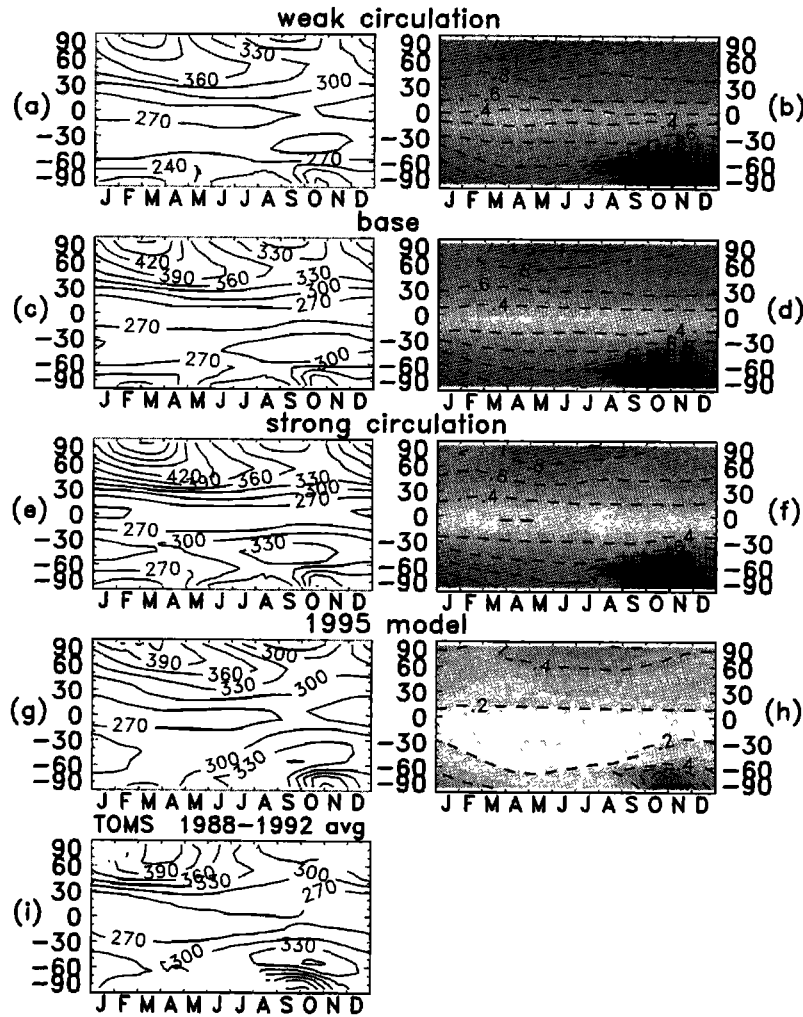


**Figure 6.** Season-latitude cross sections of reference total ozone (subsonics only, left-hand column) in Dobson units (DU), and the HSCT perturbation response in total ozone (percent change, subsonics + supersonics minus subsonics only, right-hand column) for the base scenario A, the circulation scenarios B and C, and the 1995 model transport scenario O listed in Table 1. Also included are zonal mean TOMS data averaged over 1988-1992. The contour interval is 30 DU for the left-hand column. For the right-hand column the contour intervals are 0.5% for values less (more negative) than -2%, and 0.2% for values greater (more positive) than -2%. Darkest shading corresponds to the largest negative response.

1999) and have been zonally averaged in  $10^\circ$  latitude bins from  $80^\circ\text{S}$  to  $80^\circ\text{N}$  at the standard UARS pressure levels for 100-0.1 mbar. The model results are collocated on the same latitude-pressure grid as the HALOE data. To correspond to the 1994-1999 HALOE time period, the model results have been scaled to the 1994 time-dependent  $\text{CH}_4$  boundary condition of 1.72 ppmv [WMO, 1999], which approximates a 1997 steady state boundary condition (roughly the midpoint of 1994-1999). For each scenario in Figure 5 we indicate the average difference (model minus HALOE in ppmv) and the root mean square error (RMSE) of the model compared to HALOE, after removing the average difference.

For the most part the weak circulation scenario underestimates the HALOE  $\text{CH}_4$  throughout the strato-

sphere, with the opposite occurrence for the strong circulation. With the weak circulation there is an underestimation (overestimation with the strong circulation) of methane transported from the source region at the tropical tropopause upwards in the ascending branch of the Brewer-Dobson circulation and distributed throughout the stratosphere. Figures 5c and 5d also show that the model methane is most affected by circulation changes in the middle and upper stratosphere ( $\text{CH}_4 = 0.5 - 1$  ppmv). There is decreasing sensitivity above and below this range resulting in a curvature in the scatterplots. There is little sensitivity to the model transport in the very lower stratosphere ( $> \sim 1.6$  ppmv) where  $\text{CH}_4$  is influenced primarily by the surface boundary condition. There is also relatively small sensitivity at lower mesospheric levels ( $< \sim 0.2$  ppmv) where the spatial gradi-

ents in methane are very weak. A similar pattern is seen in the other transport scenarios as will be discussed later. The base model exhibits little if any curvature and has the smallest RMSE and average difference with HALOE compared to either of the circulation scenarios. The nonzero RMSE and average difference of the base model could indicate uncertainties in the base model transport, photochemistry, and/or surface boundary condition assumptions, as well as uncertainties in the HALOE data.

In summary, we have used the available tracer data to test the sensitivity of the model simulations to variations in the residual circulation strength, and to determine an approximate range of uncertainty in the model circulation fields. Taken together, the comparisons of mean age,  $^{14}\text{C}$ ,  $\text{CH}_4$ , and the  $\text{CO}_2\text{-N}_2\text{O}$  relationship shown in Figures 1-5 suggest that the range of these data are approximately bracketed by the weak and strong circulations. These observational comparisons will be used for the other transport experiments described in later sections.

**3.1.2. High-speed civil transport (HSCT) aircraft impact.** We now discuss how these circulation scenarios affect the model simulated total ozone and HSCT impact. Figure 6 shows the reference total ozone simulation (subsonics only) on the left-hand column, along with the HSCT perturbation total ozone response (supersonics + subsonics minus subsonics only) in the right-hand column. Here we show simulations from the baseline transport scenario A and the circulation sensitivity scenarios B and C (the 1995 model will be discussed in section 3.8). The reference total ozone of the base transport compares reasonably well with the TOMS data in Figure 6i (1988-1992 average) in simulating the overall seasonal and latitudinal variations. Note that although the model simulations use source gas boundary conditions for 2015, the total  $\text{Cl}_y$  loading is very similar to 1990 conditions corresponding to the TOMS data averaged over 1988-1992.

The HSCT total ozone perturbation response of the base model (Figure 6d) is negative at all latitudes and

seasons, maximizing in the polar regions of both hemispheres during spring and summer. The largest negative response (-3.5%) occurs in the SH polar region during October. The overall negative ozone response is due to a combination of enhanced  $\text{NO}_x$  and  $\text{H}_2\text{O}$ , with the latter inducing most of the ozone loss because of increased  $\text{HO}_x$  radicals and increased occurrence of polar stratospheric clouds. The global and annual mean perturbation response of this base scenario is -0.62%, with no difference in the response averaged over the NH or SH (Table 1).

As discussed in Figure 4, simulations of  $^{14}\text{C}$ , which has a source region similar to HSCT emissions (i.e., NH middle-high latitude lower stratosphere), help illustrate how these emissions are transported throughout our model stratosphere. In Figure 7, we show the time evolution of our base transport  $^{14}\text{C}$  simulation versus latitude at 18 km, the level of peak HSCT emission. In addition to the general decay of  $^{14}\text{C}$  with time due to the imposed tropospheric loss, there is a strong seasonal cycle at middle and high latitudes of both hemispheres. Maximum mixing ratios occur during late winter and spring and are caused by downward advection of large mixing ratios as the maximum  $^{14}\text{C}$  concentrations occur above 18 km throughout most of the time period. Following the passage of the initial pulse of maximum  $^{14}\text{C}$  early in the time period, the tropics appear to be isolated from higher latitudes. This is illustrated by the low tropical  $^{14}\text{C}$  values characteristic of ascent of air from the troposphere.

This  $^{14}\text{C}$  simulation illustrates that material in the extratropical stratosphere in our model is primarily advected down from higher levels, with minimal horizontal transport through the tropics. This tropical isolation is characteristic of all stratospheric levels in our model simulation. Therefore the large negative response in total ozone in the SH polar spring in Figure 6d is primarily caused by the transport of HSCT emissions from the NH to the SH via the residual circulation, and not by horizontal mixing through the tropical stratosphere. This residual circulation mechanism advects the  $\text{NO}_x$

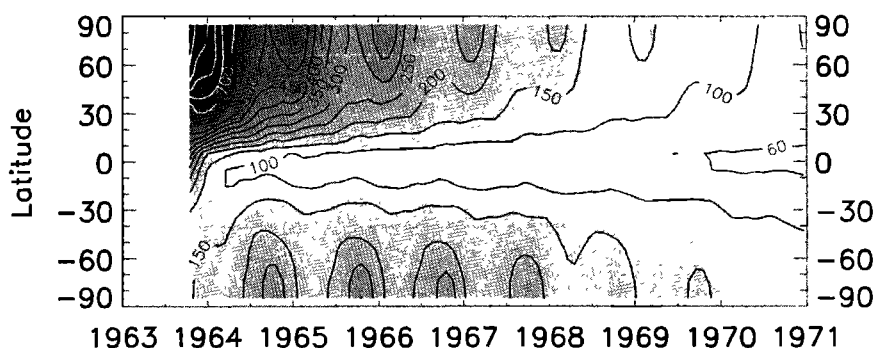


**Figure 7.** Time-latitude section of the base model time-dependent carbon 14 simulation at 18 km. Values are in mixing ratio units, defined as  $10^5$  atoms of  $^{14}\text{C}$  per gram of dry air [Kinnison *et al.*, 1994]. The contour interval is 100 for values greater than 500, and 50 for values less than 500, and includes the 60 contour level. Darkest shading corresponds to the largest values.

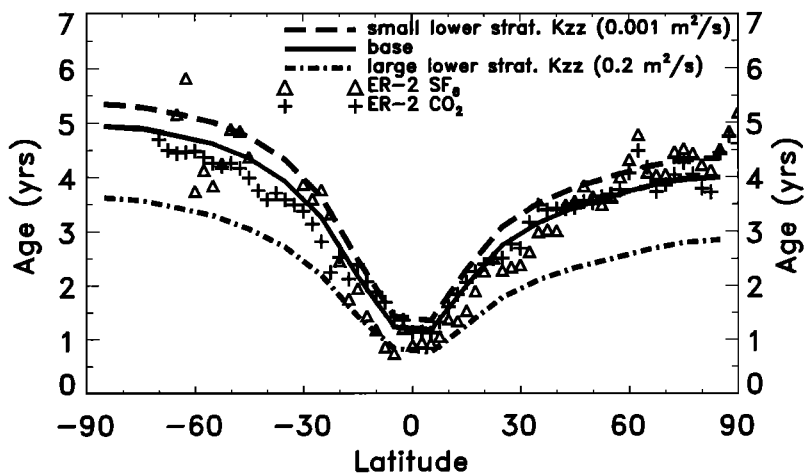


**Figure 8.** Age of air derived from model simulations of  $\text{SF}_6$  at 20 km for the base scenario A (solid line), the small lower stratospheric  $K_{zz}$  scenario D (dashed line), and the large lower stratospheric  $K_{zz}$  scenario E (dash-dot line). Also shown are age of air determined from ER-2 measurements of  $\text{SF}_6$  (triangles) and  $\text{CO}_2$  (pluses) as in Figure 1. Ages are taken relative to the tropical tropopause.

and  $\text{H}_2\text{O}$  emissions from the NH extratropical lower stratosphere upwards into the mesosphere, then horizontally to the SH, with the return descent to the lower stratosphere during winter and spring.

Returning to Figure 6 (left-hand column), the stronger circulation leads to more total ozone at high latitudes, i.e., increased downwelling, and less ozone in the tropics, with the opposite result occurring with the weaker circulation. However, because of the competing influence of dynamics and chemistry on the total ozone simulations, the overall difference with TOMS (when considering all latitudes and seasons) was only slightly better in the base model compared to either circulation scenario. This is in contrast with the tracer simulations in Figures 1-5 in which the base model was consistently in better overall agreement with the data than either scenario B or C.

The stronger (weaker) circulation results in less (more)  $\text{H}_2\text{O}$  and  $\text{NO}_y$  concentration from the HSCT emissions contained in the lower stratosphere so that the negative perturbation response in total ozone is weaker (stronger), as seen in the right-hand column of Figure 6. This is also reflected in the hemispheric and global mean total ozone responses in Table 1. The global/annual average response ranges from -0.71% to -0.53% for the weak and strong circulations, respectively. Note that in both the baseline (A) and strong circulation (C) cases, the hemispherically averaged perturbation responses are the same in the NH and SH. However, the hemispheric average response becomes increasingly asymmetric (larger in the NH) with a weakening of the circulation. It appears that with a weaker circulation, more of the emission remains confined to the NH source region, whereas increasingly stronger circulations redistribute the emissions globally leading to similar averaged responses in each hemisphere.

### 3.2. Lower Stratospheric $K_{zz}$

We have previously tested the sensitivity of lower stratospheric vertical diffusion ( $K_{zz}$ ) on our model age simulation [Fleming *et al.*, 1999]. In this section, we briefly discuss our determination of the base and upper and lower limits of this model transport parameter and how it affects the tracer simulations and HSCT perturbation response (the circulation and  $K_{yy}$  remain fixed).

Our base model tropospheric and lower stratospheric  $K_{zz}$  is based on the Brunt-Väisälä frequency squared, so that a smaller buoyancy frequency and stronger lapse rate indicative of more rapid convective overturning imply a larger value of diffusion. The minimum lower stratospheric  $K_{zz}$  is specified to be 0.01-0.02  $\text{m}^2/\text{s}$  in the tropics, following observational analyses [Hall and Waugh, 1997; Mote *et al.*, 1998], with the base  $K_{zz}$  in the extratropical lower stratosphere ranging from 0.01 to 0.05  $\text{m}^2/\text{s}$ .

We specify a lower limit  $K_{zz}$  value of 0.001  $\text{m}^2/\text{s}$  in the lower stratosphere for all latitudes and seasons (scenario D). We found that a  $K_{zz}$  smaller than 0.001  $\text{m}^2/\text{s}$  does not change the model response in the diagnostic tracers or the HSCT perturbation, so that this value appears to be the lower limit of  $K_{zz}$  in our model. Hall *et al.* [1999] recently concluded that a value of 0.1-0.2  $\text{m}^2/\text{s}$  is close to the expected upper limit on lower stratospheric  $K_{zz}$ . Therefore we adapt a value of 0.2  $\text{m}^2/\text{s}$  for all latitudes and seasons as the upper limit which gives some agreement with tracer data (scenario E). This is shown in Figure 8, which illustrates the range of mean age values simulated by these  $K_{zz}$  scenarios (see also Table 1). The observations and base model in Figure 8 are as in Figure 1. This sensitivity to  $K_{zz}$  is similar to that seen in the circulation scenarios in that a faster transport rate decreases  $\Gamma$  throughout the stratosphere and decreases the latitudinal and vertical age gradients,

with material removed from the stratosphere at a faster rate. Figure 8 is representative of the general tracer sensitivity to  $K_{zz}$ , as analogous results are seen in the vertical age profiles, the CO<sub>2</sub>-N<sub>2</sub>O correlation, and the <sup>14</sup>C simulation (not shown).

We found that the model reference total ozone field and the model CH<sub>4</sub> comparison with HALOE data were relatively insensitive to varying the lower stratospheric  $K_{zz}$ . In fact, increasing the vertical diffusion to an unrealistically large value of 1 m<sup>2</sup>/s does not appreciably change the reference total ozone simulation compared to that obtained with the small  $K_{zz}=0.001$  m<sup>2</sup>/s, even though the distribution of  $\Gamma$  is severely affected [Fleming et al., 1999]. This is likely due to the fact that total column ozone is a vertically integrated quantity which is not strongly affected by changes in vertical diffusion. However as indicated in Table 1, the HSCT perturbation response in total ozone exhibits a relatively large variation with  $K_{zz}$ . Consistent with the tracer simulations, a larger  $K_{zz}$  flushes more of the HSCT emission out of the lower stratosphere into the troposphere leading to a weaker negative response in total ozone.

Consistent with the  $\Gamma$  simulations, Table 1 shows that for the smallest  $K_{zz}$  of 0.001 m<sup>2</sup>/s, the NH, SH, and global/annual mean responses are only slightly enhanced compared to the base case, whereas the large  $K_{zz}$  scenario (0.2 m<sup>2</sup>/s) gives significantly weaker negative total ozone responses at all latitudes relative to the base scenario. Interestingly, the large  $K_{zz}$  scenario gave a larger response averaged over the NH than the SH, with the small  $K_{zz}$  case showing the opposite hemispheric asymmetry. This is in contrast with the circulation scenarios in which the weaker transport produced a greater averaged response in the NH than in the SH.

### 3.3. Mesospheric Gravity Wave Effects

The model gravity wave parameterization [Lindzen, 1981; Holton and Zhu, 1984] computes wave drag and vertical diffusion in the upper stratosphere and mesosphere, with the wave drag having a direct effect on the residual circulation. To evaluate the stratospheric effects of uncertainties in the gravity wave parameterization and related input parameters, we ran two additional scenarios with weak and strong mesospheric gravity wave-induced drag and diffusion (scenarios F and G).

Despite simulating large changes in mesospheric water vapor and some substantial differences in upper stratospheric/lower mesospheric methane compared with HALOE, these gravity wave scenarios had only a small influence on tracer distributions in the lower and middle stratosphere in our model. Below 35 km, the changes in global/annual mean age between scenarios F and G were at most 4-8 months (Table 1), with only very small changes in the model simulations of <sup>14</sup>C. Consistent with this, the hemispheric and global mean total ozone perturbation response also had relatively small changes, as shown in Table 1.

### 3.4. Global Stratospheric $K_{yy}$

The irreversible horizontal mixing induced by large scale eddy processes in the stratosphere is generally represented as an eddy diffusion ( $K_{yy}$ ) in 2-D models. This parameterization can be a significant source of model uncertainty. Our model derives this diffusion parameter from potential vorticity (PV) using the flux-gradient relationship such that  $K_{yy}$  is taken as the ratio of the zonal mean PV flux to the latitudinal gradient of zonal mean PV [Newman et al., 1988; Randel and Garcia, 1994]. The PV flux, or the Eliassen-Palm (E-P) flux divergence, is computed from 3-D meteorological analyses [e.g., Andrews et al., 1987] and provides a diagnostic estimate of the planetary wave drag. This quantity is used to compute the model  $K_{yy}$  and residual circulation fields self-consistently, and uncertainties in the E-P flux derivation will affect these model transport parameters simultaneously. This coupling will be addressed in section 3.5. Deriving the E-P flux and  $K_{yy}$  can be especially uncertain in the tropics, where estimating winds is problematic. This will be discussed separately in section 3.7. In this section, we examine the model sensitivity to changes in  $K_{yy}$  alone, with the circulation and  $K_{zz}$  parameters unchanged. This addresses the general uncertainty in using PV and the flux-gradient relationship to derive the zonal mean mixing rate of chemically active species throughout the stratosphere.

Figures 9 and 10 show distributions of mean age for scenarios in which  $K_{yy}$  was decreased (H) and increased (I) by a constant factor of 2 everywhere above the tropopause. Again the base model and observations are as in Figures 1 and 2; the 1995 model scenario in Figure 9 (dotted line) will be discussed in section 3.8. These  $K_{yy}$  scenarios generally bracket the age observations. Although the large  $K_{yy}$  scenario appears to be older than observations in the tropics, it is close to the OMS data at midlatitudes (Figure 10). Also, the small  $K_{yy}$  scenario is reasonable in the tropics, but gives simulated ages that are significantly younger than the CWAS or OMS ages at midlatitudes.

Qualitatively, increasing the horizontal diffusion reduces the latitudinal gradients in  $\Gamma$  and increases the mean age throughout the stratosphere, with this latter tendency increasing with altitude (see also Table 1). This  $\Gamma$  dependence on horizontal mixing is due to the fact that with larger  $K_{yy}$ , air parcels undergo more recycling through the middle atmosphere via ascent in the tropics and descent in the extratropics, before returning to the troposphere, and hence achieve an older mean age [e.g., Bacmeister et al., 1998; Hall et al., 1999]. As a result, the vertical gradients in  $\Gamma$  throughout the stratosphere increase with increasing  $K_{yy}$  as seen in Figure 10. The weak vertical gradients in the extratropics in the small  $K_{yy}$  scenario likely illustrate the dominance of the residual circulation, which is primarily downward in this region, in controlling the long lived tracer distributions in this case. We note that a similar overall sensitivity to  $K_{yy}$  is seen in the CO<sub>2</sub>-N<sub>2</sub>O correlation

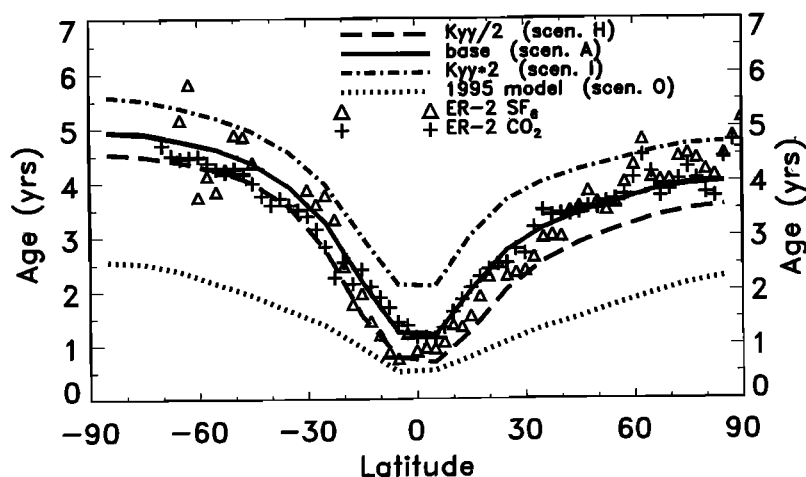


**Figure 9.** Age of air derived from model simulations of SF<sub>6</sub> at 20 km for the base scenario A (solid line), the small global  $K_{yy}$  scenario H (dashed line), the large global  $K_{yy}$  scenario I (dash-dot line), and the 1995 transport scenario O (dotted line). Also shown are age of air determined from ER-2 measurements of SF<sub>6</sub> (triangles) and CO<sub>2</sub> (pluses) as in Figure 1. Ages are taken relative to the tropical tropopause.

and the <sup>14</sup>C simulation (not shown), with a smaller  $K_{yy}$  resulting in <sup>14</sup>C being removed from the stratosphere at a faster rate.

Referring back to the model-HALOE CH<sub>4</sub> scatterplots in Figure 5, both  $K_{yy}$  scenarios (H and I) result in a larger scatter (RMSE) and average difference compared to the base model. The  $K_{yy}$  scenarios also exhibit a curvature pattern similar to the circulation scenarios. Methane is most sensitive to the rate of transport in the middle stratosphere (CH<sub>4</sub> values ~1 ppmv), with a decreasing sensitivity away from this level. The large  $K_{yy}$  scenario primarily underestimates CH<sub>4</sub> relative to HALOE, with the opposite occurrence for the small  $K_{yy}$

case. With increased horizontal mixing, more CH<sub>4</sub> is transported away from the tropical ascending branch of the Brewer-Dobson circulation toward high latitudes where the vertical motion is downward, giving smaller methane concentrations compared to HALOE throughout most of the stratosphere.

For the reference and perturbation responses in total ozone (figures not shown), decreasing  $K_{yy}$  increases the latitudinal gradients, and more of the HSCT emission remains confined near the NH source region so that the ozone perturbation response at NH high latitudes becomes larger. South of ~40°N, the perturbation response increases with increasing diffusion as more of the emission is flushed out to the tropics and into the SH. Since the HSCT emissions originate primarily at NH middle and high latitudes, changing  $K_{yy}$  does not strongly affect the overall NH average (Table 1). In contrast, the SH and global averages are enhanced dramatically with increased horizontal mixing. The global average total ozone response dependence on  $K_{yy}$  is consistent with the mean age and <sup>14</sup>C dependence discussed above.

### 3.5. Self-Consistent $K_{yy}$ and Circulation Changes

Uncertainties in the E-P flux divergence calculation affect both the  $K_{yy}$  and residual circulation in a self-consistent manner. To investigate this sensitivity, we included an additional scenario in which  $K_{yy}$  has been decreased by a factor of 2 as in scenario H, along with a corresponding factor of 2 decrease in the wave drive above the tropopause, which weakens the circulation. We also included a case in which both  $K_{yy}$  and the wave drive were increased by a factor of 2 above the tropopause. These are listed as scenarios J and K in Table 1.

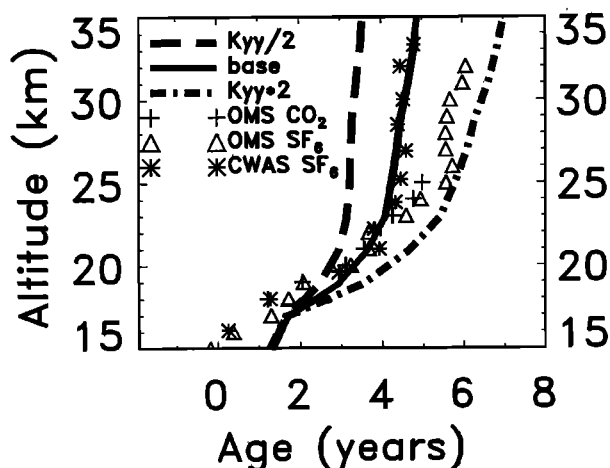


**Figure 10.** Vertical profiles of age of air derived from model simulations of SF<sub>6</sub> for the base scenario A (solid line), the small global  $K_{yy}$  scenario H (dashed line), and the large global  $K_{yy}$  scenario I (dash-dot line) at 40°N. Also shown are age of air determined from balloon measurements of SF<sub>6</sub> and CO<sub>2</sub> as in Figure 2b. Ages are taken relative to the tropical tropopause.

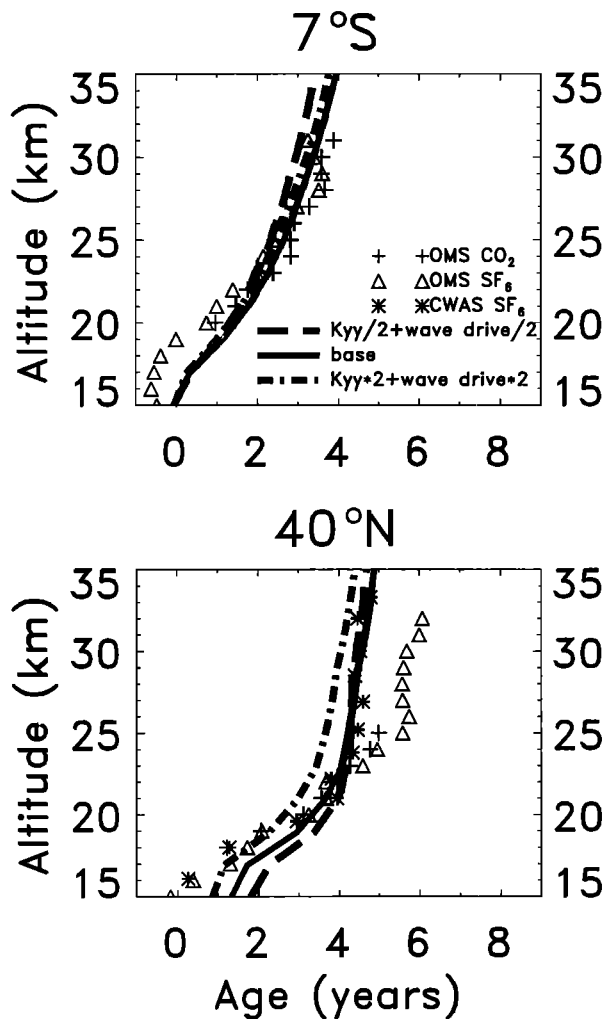


**Figure 11.** Vertical profiles of age of air derived from model simulations of SF<sub>6</sub> for the base scenario A (solid line), and the combined  $K_{yy}$  + wave drive scenarios J (dashed line) and K (dash-dot line) listed in Table 1 and discussed in the text. Also shown are age of air determined from balloon measurements of SF<sub>6</sub> and CO<sub>2</sub> as in Figure 2. Ages are taken relative to the tropical tropopause.

The age of air responses to these scenarios are illustrated in Figure 11. We do not show results at high latitudes since the relative responses are very similar to those at 40°N (consistent results are also revealed in the <sup>14</sup>C and CO<sub>2</sub> – N<sub>2</sub>O simulations and are not shown). While decreasing only  $K_{yy}$  gives substantially younger  $\Gamma$  throughout the stratosphere (Figures 9 and 10), Figure 11 (dashed line) shows that including the corresponding reduction in the wave driven circulation counteracts this effect. The net result in the extratropics is that the ages are slightly older below 20 km, and very similar above 20 km relative to the base model (see also Table 1). This cancellation of effects is also seen in scenario K (dashed-dotted line). Although in this case, the increased circulation more than compensates for the increased diffusion so that the net result gives slightly

younger  $\Gamma$  relative to the base case poleward of  $\sim \pm 15^\circ$  to  $20^\circ$ . In the tropics, both scenarios J and K give very similar  $\Gamma$ , so that the latitudinal age gradients in the subtropics are somewhat larger in scenario J, especially in the lower stratosphere.

Consistent with these changes in  $\Gamma$ , scenario J gives the same global/annual mean perturbation total ozone response as the base case (-0.62%), while scenario K slightly diminishes the response (-0.53%). The combination of a weaker circulation and diffusion gives a larger response in the NH, as it does when these transport components are decreased separately (scenarios B and H). This hemispheric asymmetry is reversed when both the circulation and  $K_{yy}$  are increased, and comparison of scenarios C and I indicate that the diffusion increases are primarily responsible for giving a greater response in the SH in scenario K.

### 3.6. Cross-Tropopause $K_{yy}$

We also investigated the model response to changes in horizontal diffusion across the tropopause. Recent assessment reports have noted the importance of cross-tropopause transport in model simulations of HSCT emissions [Kawa *et al.*, 1999; Park *et al.*, 1999]. It was suggested that 2-D and 3-D models simulate a different correlation between mean age and NO<sub>y</sub> accumulation. This is perhaps due to the inherent differences between 2-D and 3-D model formulations of cross-tropopause transport, which can have large zonal asymmetries. Also, Hall and Waugh [2000] suggested that there is a general tendency for more mixing between the upper troposphere and lower stratosphere in 3-D. In our 2-D model the tropopause, which is a function of latitude and season and is based on NCEP data, separates very fast and very slow vertical mixing ( $K_{zz}$ ) regimes. There is also cross-tropopause transport horizontally via the  $K_{yy}$  field where the tropopause height changes with latitude. This occurs primarily at midlatitudes between  $\pm 25^\circ$  and  $60^\circ$ .

To test how this horizontal transport affects the model simulations, we computed an additional scenario (L) in which the cross-tropopause  $K_{yy}$  values were significantly increased over the base model (the  $K_{zz}$  and circulation remain unchanged). However, the resulting tracer simulations changed only slightly from the baseline case, and mean ages were at most 2 months older throughout the stratosphere. Similarly, the total ozone perturbation response was virtually unchanged compared to scenario A (Table 1). This illustrates the very small sensitivity to the rate of horizontal cross-tropopause diffusive transport in our model simulations.

### 3.7. Tropical Stratospheric $K_{yy}$

Properly quantifying the rate of horizontal mixing in the tropical stratosphere is particularly important for HSCT simulations. This mixing rate directly affects how much aircraft exhaust is transported from the mid-

latitude source region into the tropics, where it can be transported upward via the residual circulation to the middle stratosphere and greatly increase the amount of ozone destruction incurred.

Previous studies have examined the influence of horizontal mixing between the tropics and midlatitudes [e.g., *Plumb*, 1996; *Neu and Plumb*, 1999]. In their model study of HSCT perturbations, *Shia et al.* [1998] adjusted their tropical  $K_{yy}$  values to match the tropical-midlatitude exchange rates estimated from measurements of chemical species by *Volk et al.* [1996] and *Schoeberl et al.* [1997]. Their resulting tropical stratospheric  $K_{yy}$  values ranged from 0.07 to  $0.13 \times 10^6$  m<sup>2</sup>/s. This “leaky pipe” model represented an intermediate level of diffusivity compared to the “tropical pipe” model, i.e., extreme tropical isolation, and the “global diffuser” model [*Plumb*, 1996].

In our model, computing  $K_{yy}$  from the E-P flux divergence via the flux-gradient calculation can be particularly uncertain in the tropics where quantifying the zonal and meridional winds is problematic. To derive our base model E-P flux divergence and  $K_{yy}$  in the tropical stratosphere, we use zonal and meridional winds measured by the high resolution Doppler imager (HRDI) on board UARS averaged over 1992 to 1996, along with temperature data from the National Centers for Environmental Prediction (NCEP) analyses for the same time period. Our base model  $K_{yy}$  field in this region varies spatially and seasonally. The annual mean, area weighted average  $K_{yy}$  for 15°S–15°N decreases from  $0.14 \times 10^6$  m<sup>2</sup>/s just above the tropopause to  $0.07 \times 10^6$  m<sup>2</sup>/s at 23 km, and then gradually increases to  $0.1 \times 10^6$  m<sup>2</sup>/s at 29 km and  $0.3 \times 10^6$  m<sup>2</sup>/s at 50 km. These values are similar to those of the “leaky pipe” model of *Shia et al.* [1998]. We also note that our base model tropical E-P flux and  $K_{yy}$  quantities obtained from the HRDI and NCEP data are generally similar to those derived from the United Kingdom Meteorological Office (UKMO) stratospheric assimilation fields [*Swinbank and O’Neill*, 1994].

To test the sensitivity of our model simulations to the rate of tropical horizontal diffusion, we specified a very small constant  $K_{yy}$  of  $0.01 \times 10^6$  m<sup>2</sup>/s throughout the tropical stratosphere (15°S–15°N, 15–50 km) for all seasons in scenario M. This value is the lower limit of  $K_{yy}$  in our model and is a bit smaller than the  $0.03 \times 10^6$  m<sup>2</sup>/s lower stratospheric value used in the tropical pipe model of *Shia et al.* [1998]. Scenario M results in an extremely isolated tropical region with very large tracer gradients between the tropics and midlatitudes. The resulting vertical age profiles are very similar to the  $K_{yy}/2$  case (scenario H) shown in Figure 10, with little or no vertical gradient in the extratropics above 21 km (see also Table 1).

For the large tropical  $K_{yy}$  case we specified a constant value of  $0.2 \times 10^6$  m<sup>2</sup>/s over the 15°S–15°N, 15–50 km region for all seasons in scenario N. This value was chosen to be somewhat larger than that inferred

from constituent data for the leaky pipe model of *Shia et al.* [1998], but smaller than the  $0.3 \times 10^6$  m<sup>2</sup>/s tropical value used in the *Shia et al.* global diffuser model. Also, scenario N gave tropical-midlatitude CH<sub>4</sub> gradients that were somewhat weaker than observed in HALOE data [e.g., *Randel et al.*, 1998]. We therefore expect this scenario to be close to the upper limit of realistic tropical  $K_{yy}$  in our model.

In addition to the weaker subtropical tracer gradients, scenario N gives slightly older mean ages throughout most of the stratosphere relative to the base case, consistent with the global  $K_{yy}$  increase in scenario I. This difference increases with altitude and is largest (7 months) in the tropical upper stratosphere. Overall, the simulated  $\Gamma$  in this scenario is well within the limits of observations. We note that the E-P flux divergence in the tropical stratosphere in the base model is inherently small, so that changing this quantity and the circulation to be dynamically consistent with the  $K_{yy}$  changes in scenarios M and N gave very similar results to those obtained by changing  $K_{yy}$  only.

As seen in Table 1, the total ozone response tendencies in these tropical diffusion cases are generally similar to those seen in the global  $K_{yy}$  scenarios H and I. The NH average response is significantly less sensitive to the tropical horizontal mixing rate than is the SH average, as the latter increases from -0.46% to -0.74% between scenarios M and N. The resulting global average response also increases with increasing tropical diffusion, which is qualitatively consistent with the modeling results of *Shia et al.* [1998]. The global perturbation response ranges from -0.53% to -0.68% in scenarios M and N, which is a somewhat smaller range than in the circulation,  $K_{zz}$ , or global  $K_{yy}$  scenarios.

We note finally that although the SH response is diminished with the small tropical diffusion, it is still significant throughout the year. This is consistent with the <sup>14</sup>C simulation in Figure 7, illustrating that much of the interhemispheric transport of HSCT emissions in our base model occurs via the seasonal ascending and descending branches of the stratospheric-mesospheric residual circulation, with horizontal diffusive transport through the tropical stratosphere being of secondary importance.

### 3.8. The 1995 Model Transport

The previous 1995 version of our model transport was used in the 1995 NASA HSCT assessment [*Stolarski et al.*, 1995]. As discussed by *Fleming et al.* [1999], our 1999 model transport (base scenario A) simulates tracers that are in significantly better agreement with observations compared to this previous model version. As seen in Figure 9, the gradients and absolute values of  $\Gamma$  in the 1995 model (scenario O) are significantly underestimated relative to observations. The annual/global mean ages are the youngest of all the simulations performed in this study, and are much younger throughout the stratosphere compared with scenario A (Table

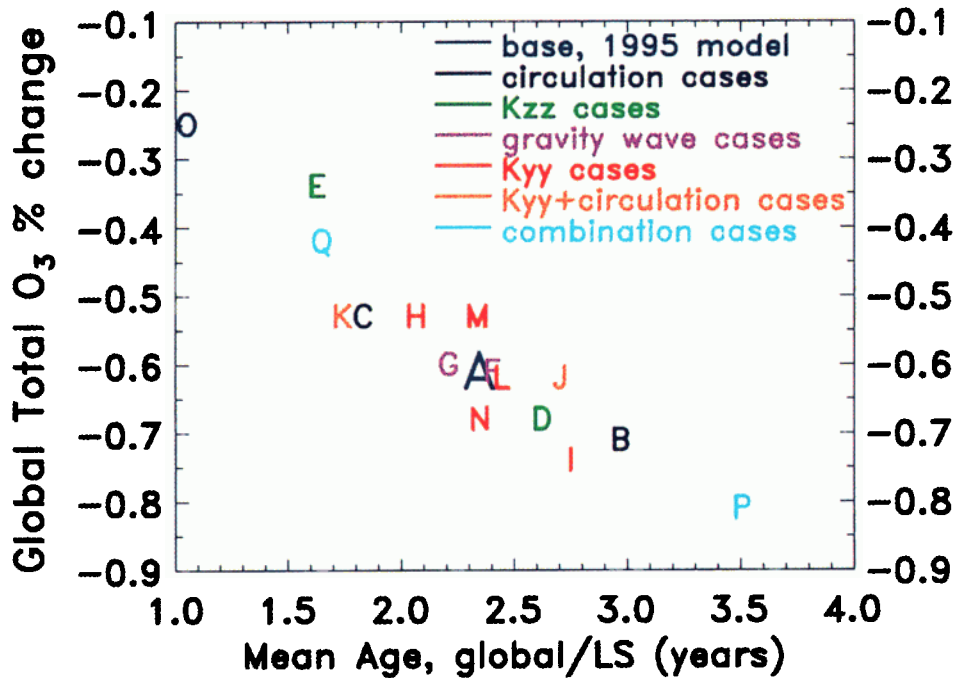


**Plate 1.** Scatterplot of the annual and globally averaged perturbation response in total ozone (percent change, subsonics + supersonics minus subsonics only), versus the annual, global, and pressure weighted average mean age (years) for the lower stratosphere (LS=16-22 km), for all model transport scenarios listed in Table 1. Letters for each scenario are color coded according to the type of transport variation imposed, as indicated in the legend.

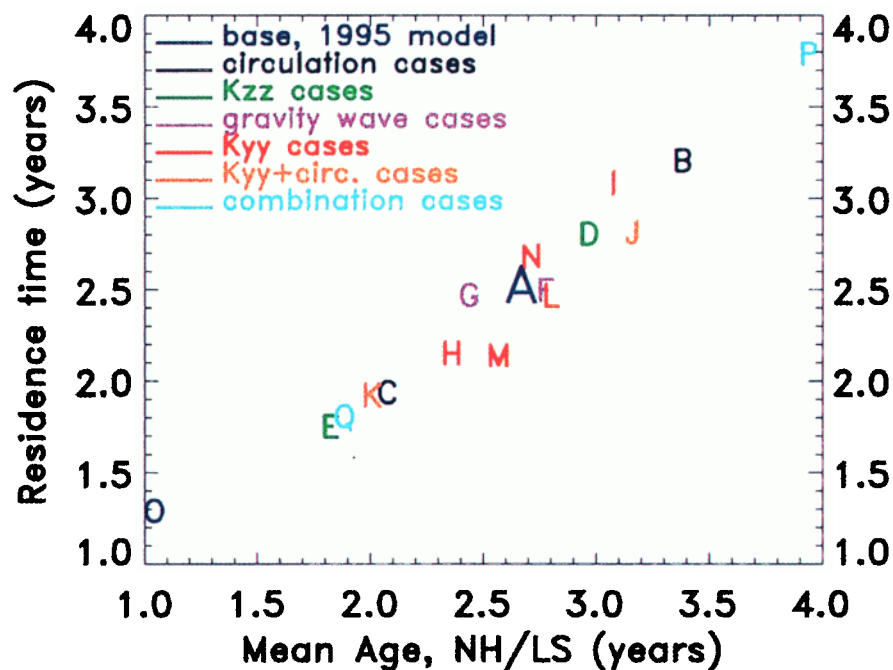


**Plate 2.** Scatterplot of residence time ( $\tau_R$ ) versus the annual and pressure weighted average mean age (years) for the Northern Hemisphere midlatitude lower stratosphere (NH/LS=35°N-55°N, 16-22 km), for all model transport scenarios listed in Table 1. Letters for each scenario are color coded according to the type of transport variation imposed, as indicated in the legend. See text for discussion of  $\tau_R$ .

1). This is primarily due to overly strong circulation and vertical mixing rates in certain regions in the older model version. There is also improper resolving of diffusion changes across regions that have differing transport characteristics, e.g., changes in vertical mixing across the tropopause and horizontal mixing between the tropics and midlatitudes. These inaccuracies in the 1995 model transport are also revealed in the model-HALOE CH<sub>4</sub> scatterplot in Figure 5b. It is clear that this model version exhibits a much larger scatter and average difference with HALOE compared to the base 1999 model transport at most levels of the stratosphere.

In contrast, the reference total ozone simulation with the 1995 transport (Figure 6g) is reasonably similar overall to the TOMS data, and compares better with TOMS than does the base model during some seasons and latitudes. As the tracer comparisons provide a rigorous test of model transport, the good agreement of the 1995 model with the TOMS data should be regarded as fortuitous. This illustrates how model transport deficiencies that are illuminated in inert tracer simulations can be hidden in a vertically integrated and chemically active quantity such as total column ozone.

Such transport deficiencies can ultimately cause significant biases in the model simulated response to a lower stratospheric perturbation such as HSCT emissions. This is revealed in the 1995 model ozone perturbation in Figure 6h. Compared with the base case, the 1995 model response is significantly weaker at all latitudes and seasons, consistent with the overly fast transport rates revealed in the age of air simulations. The annual and global mean total ozone response with the 1995 model transport is -0.25% compared to -0.62% in the base case.

### 3.9. Age of Air Versus Total Ozone Perturbation Response

Plate 1 shows the correlation of mean age with the total ozone perturbation response for the 17 transport scenarios listed in Table 1. Here we plot the global, annual and pressure weighted average of  $\Gamma$  over the 16-22 km region against the global and annual mean perturbation total ozone responses. There is a strong correlation between the mean age and total ozone response, such that a younger age implies less emission accumulation and less ozone loss. It also appears that the correlation is generally independent of the type of transport change imposed. Exceptions are the gravity wave scenarios (F and G) which show virtually no change in total ozone response, but exhibit some change in lower stratospheric  $\Gamma$  due to significant circulation and  $K_{zz}$  changes in the upper stratosphere and mesosphere. Also, the tropical  $K_{yy}$  dependence (scenarios M and N) shows a moderate change in the total ozone response, but little if any change in  $\Gamma$  at these altitudes (16-22 km), although we note that changes in tropical diffusion induce significant changes in mean age in the middle and upper

stratosphere (Table 1). Plate 1 illustrates again that the 1995 transport (scenario O) gives significantly younger ages and a much weaker total ozone response compared to the other transport scenarios.

Plate 1 and Table 1 show two additional scenarios in which the circulation strength, global  $K_{yy}$ , and  $K_{zz}$  fields are changed simultaneously to increase the stratospheric age and residence time, i.e., the circulation and  $K_{zz}$  are decreased and the  $K_{yy}$  is increased (scenario P). Opposite changes are made to decrease the age and residence time in scenario Q. Although the resulting mean ages are outside of the range of observations, we show these cases to demonstrate that the resulting correlation between  $\Gamma$  and the total ozone response is similar to that when changing the different transport components separately. This demonstrates that the model response remains linear and does not change qualitatively when imposing a combination of transport changes.

Throughout this paper we have assumed that mean age, which has been extensively observed, is a proxy for the HSCT emission residence time ( $\tau_R$ ) which is not directly observable. Following *Hall and Waugh* [2000], we test this by computing  $\tau_R$  from a steady state simulation of NO<sub>y</sub> calculated as a passive tracer with a specified tropospheric loss (the “A3” transport experiment used in the recent Models and Measurements Intercomparison Project II (MMII) [*Park et al.*, 1999]). The emissions are global, but are input primarily at NH midlatitudes, and correspond to 500 HSCTs at Mach 2.4, with E.I.=10.  $\tau_R$  is taken as the ratio of the resulting annually averaged total NO<sub>y</sub> mass above the tropopause to the rate of input of NO<sub>y</sub> mass above the tropopause. The resulting relationship between  $\tau_R$  and mean age is shown in Plate 2 (the color coding is as in Plate 1). Here we plot the area and pressure-weighted annual average of  $\Gamma$  over the region of peak HSCT emission in the midlatitude NH lower stratosphere (35°N-55°N, 16-22 km). These results are consistent with Plate 1. A younger mean age implies a shorter  $\tau_R$  and there is a generally strong correlation between these parameters among most of the scenarios. Again, the notable exceptions are the tropical  $K_{yy}$  scenarios (M and N) and the gravity wave scenarios (F and G) as discussed above.

## 4. Conclusions

We have examined the sensitivity of stratospheric tracers and an HSCT aircraft perturbation to potential uncertainties in 2-D model empirical transport fields. These uncertainties can arise from a variety of sources, including the algorithms, assumptions, and/or data sets used to derive the model transport components. We estimate these uncertainties by varying the transport parameters so that the range of model tracer simulations brackets the observations. This range varies with transport parameter. For example, the range of residual circulation velocities is constrained by observations to

be within 25% of the base circulation, while the range of global stratospheric  $K_{yy}$  rates is observationally constrained to be within a factor of 2 of the base.

We find a strong linear correlation between mean age, the emission residence time, and the HSCT perturbation response in total ozone among most of the transport scenarios performed, demonstrating a tight relationship between age of air and the HSCT impact. Increasing the residual circulation or lower stratospheric  $K_{zz}$  decreased the mean age and emission residence time, and diminished the negative ozone response to HSCTs. Increasing the global stratospheric  $K_{yy}$  had the opposite effect by increasing the residence time and mean age via greater recycling of air through the middle atmosphere, and enhancing the global mean total ozone HSCT response. Also, the vertical gradients in  $\Gamma$  throughout the stratosphere were significantly reduced with large scale reductions in horizontal diffusion. This likely illustrates the dominance of the residual circulation in controlling the long lived tracer distributions with relatively small global  $K_{yy}$  values.

Uncertainties in the mechanical wave forcing (E-P flux) calculation affect both the  $K_{yy}$  and residual circulation simultaneously, and incorporating these variations self-consistently had a cancellation effect. In this case, the circulation changes had a somewhat larger impact than the  $K_{yy}$  changes in determining the net mean age and perturbation responses globally.

Variations in the tropical stratospheric  $K_{yy}$  gave qualitatively similar results to the global  $K_{yy}$  variations. However, these scenarios resulted in a somewhat smaller range of uncertainty in the model  $\Gamma$  and total ozone response relative to the other transport uncertainties. Also, the model simulations below 35 km showed relatively small sensitivity to the strength of the mesospheric gravity wave drag and diffusion, and to the magnitude of the horizontal diffusive transport across the tropopause.

The base model transport provides the most favorable overall comparison with the tracer data, and simulates a steady state global and annual mean HSCT perturbation response in total ozone of -0.62%, assuming a  $\text{NO}_x$  emission index of 5 g/kg, 500 airplanes, and a 10% gas-to-particle conversion of the  $\text{SO}_2$  emission. Variations in lower stratospheric  $K_{zz}$  gave the largest range of responses in total ozone, as the direct removal of emissions from the stratosphere is most sensitive to this parameter. For scenarios having tracer distributions in reasonable agreement with measurements (excluding scenarios O, P, and Q), the global total ozone response ranged from -0.34% to -0.74%. This range is significantly smaller than the general uncertainty estimates that consider model differences and a variety of atmospheric processes, as given in the recent assessment reports [Kawa *et al.*, 1999; IPCC, 1999].

The base model global total ozone response of -0.62% is significantly larger than the -0.25% simulated by our

previous model used in the 1995 HSCT assessment. Although the reference total ozone simulated by this 1995 model transport is in reasonable agreement with TOMS data, the corresponding tracer simulations reveal that the 1995 model transport rates were substantially different than indicated by observations. This illustrates that the 1995 model-data agreement in total ozone is fortuitous and that model transport deficiencies, which are evident in inert tracer comparisons, can be hidden in a vertically integrated and chemically active quantity such as total ozone. Such model inaccuracies ultimately cause significant biases in the simulated ozone response to an HSCT perturbation.

**Acknowledgments.** We thank D. Waugh for helpful discussions and A. Andrews for providing the OMS  $\text{CO}_2$  ages. We also thank the NASA Atmospheric Chemistry Modeling and Analysis Program and the UARS Science Investigation Program for support of this project.

## References

- Andrews, A.E., K.A. Boering, B.C. Daube, S.C. Wofsy, E.J. Hintsa, E.M. Weinstock, and T.P. Bui, Empirical age spectra for the lower tropical stratosphere from in situ observations of  $\text{CO}_2$ : Implications for stratospheric transport, *J. Geophys. Res.*, **104**, 26,581-26,595, 1999.
- Andrews, A.E., K.A. Boering, S.C. Wofsy, B.C. Daube, D.B. Jones, S. Alex, M. Loewenstein, J.R. Podolske, and S.E. Strahan, Empirical age spectra for the midlatitude lower stratosphere from in situ observations of  $\text{CO}_2$ : Quantitative evidence for a subtropical "barrier" to horizontal transport, *J. Geophys. Res.*, in press, 2000.
- Andrews, D.G., J.R. Holton, and C.B. Leovy, *Middle Atmosphere Dynamics*, 498 pp., Academic, San Diego, Calif., 1987.
- Bacmeister, J.T., D.E. Siskind, M.E. Summers, S.D. Eckermann, Age of air in a zonally averaged two-dimensional model, *J. Geophys. Res.*, **103**, 11,263-11,288, 1998.
- Boering, K.A., S.C. Wofsy, B.C. Daube, H.R. Schneider, M. Loewenstein, J.R. Podolske, and T.J. Conway, Stratospheric mean ages and transport rates from observations of carbon dioxide and nitrous oxide, *Science*, **274**, 1340-1343, 1996.
- Conway, T.J., P.P. Tans, L.S. Waterman, K.W. Thoning, D.R. Kitzis, K.A. Masarie, and N. Zhang, Evidence for interannual variability of the carbon cycle from the NOAA Climate Monitoring and Diagnostics Laboratory Global Air Sampling Network, *J. Geophys. Res.*, **99**, 22,831-22,855, 1994.
- Douglass, A.R., C.H. Jackman, and R.S. Stolarski, Comparison of model results transporting the odd nitrogen family with results transporting separate odd nitrogen species, *J. Geophys. Res.*, **94**, 9862-9872, 1989.
- Elkins, J.W., et al., Airborne gas chromatograph for in situ measurements of long-lived species in the upper troposphere and lower stratosphere, *Geophys. Res. Lett.*, **23**, 347-350, 1996.
- Fleming, E.L., C.H. Jackman, R.S. Stolarski, and D.B. Conside, Simulation of stratospheric tracers using an improved empirically-based two-dimensional model transport formulation, *J. Geophys. Res.*, **104**, 23,911-23,934, 1999.
- Garcia, R.R., and S. Solomon, A numerical model of the zonally averaged dynamical and chemical structure of the

- middle atmosphere, *J. Geophys. Res.*, *88*, 1379-1400, 1983.
- Garcia, R.R., F. Stordal, S. Solomon, and J.T. Kiehl, A new numerical model of the middle atmosphere, 1, Dynamics and transport of tropospheric source gases, *J. Geophys. Res.*, *97*, 12,967-12,991, 1992.
- Geller, L.S., J.W. Elkins, J.M. Lobert, A.D. Clarke, D.F. Hurst, J.H. Butler, and R.C. Myers, Tropospheric SF<sub>6</sub>: Observed latitudinal distribution and trends, derived emissions and interhemispheric exchange time, *Geophys. Res. Lett.*, *24*, 675-678, 1997.
- Hall, T.M., and D.W. Waugh, Tracer transport in the tropical stratospheric due to vertical diffusion and horizontal mixing, *Geophys. Res. Lett.*, *24*, 1383-1386, 1997.
- Hall, T.M., and D.W. Waugh, Influence of nonlocal chemistry on tracer distributions: Inferring the mean age of air from SF<sub>6</sub>, *J. Geophys. Res.*, *103*, 13,327-13,336, 1998.
- Hall, T.M., and D.W. Waugh, Stratospheric residence time and its relationship to mean age, *J. Geophys. Res.*, *105*, 6773-6782, 2000.
- Hall, T.M., D.W. Waugh, K.A. Boering, and R.A. Plumb, Evaluation of transport in stratospheric models, *J. Geophys. Res.*, *104*, 18,815-18,839, 1999.
- Harnisch, J., R. Borchers, P. Fabian, and M. Maiss, Tropospheric trends for CF<sub>4</sub> and C<sub>2</sub>F<sub>6</sub> since 1982 derived from SF<sub>6</sub> dated stratospheric air, *Geophys. Res. Lett.*, *23*, 1099-1102, 1996.
- Holton, J.R., and X. Zhu, A further study of gravity wave induced drag and diffusion in the mesosphere, *J. Atmos. Sci.*, *41*, 2653-2662, 1984.
- Intergovernmental Panel on Climate Change (IPCC), *Special Report on Aviation and the Global Atmosphere*, Cambridge University Press, Cambridge, UK, 1999.
- Jackman, C.H., A.R. Douglass, R.B. Rood, R.D. McPeters, and P.E. Meade, Effect of solar proton events on the middle atmosphere during the past two solar cycles as computed using a two-dimensional model, *J. Geophys. Res.*, *95*, 7417-7428, 1990.
- Jackman, C.H., A.R. Douglass, K.F. Brueske, and S.A. Klein, The influence of dynamics on two-dimensional model results: Simulations of <sup>14</sup>C and stratospheric NO<sub>x</sub> injections, *J. Geophys. Res.*, *96*, 22,559-22,572, 1991.
- Jackman, C.H., E.L. Fleming, S. Chandra, D.B. Considine, and J.E. Rosenfield, Past, present, and future modeled ozone trends with comparisons to observed trends, *J. Geophys. Res.*, *101*, 28,753-28,767, 1996.
- Jackman, C.H., D.B. Considine, and E.L. Fleming, A global modeling study of solid rocket aluminum oxide emission effects on stratospheric ozone, *Geophys. Res. Lett.*, *25*, 907-910, 1998.
- Kawa, S.R. et al., Editors, Assessment of the Effects of High Speed Aircraft in the Stratosphere: 1998, *NASA Ref. Publ.*, *NASA/TM-1999-209237*, 1999.
- Kinnison, D.E., H.S. Johnston, and D.J. Wuebbles, Model study of atmospheric transport using carbon 14 and strontium 90 data as inert tracers, *J. Geophys. Res.*, *99*, 20,647-20,664, 1994.
- Li, S., and D.W. Waugh, Sensitivity of mean age and long-lived tracers to transport parameters in a two-dimensional model, *J. Geophys. Res.*, *104*, 30,559-30,569, 1999.
- Lindzen, R. S., Turbulence and stress owing to gravity wave and tidal breakdown, *J. Geophys. Res.*, *86*, 9707-9714, 1981.
- Mote, P.W., T.J. Dunkerton, M.E. McIntyre, E.A. Ray, P.H. Haynes, and J.M. Russell III, Vertical velocity, vertical diffusion, and dilution by midlatitude air in the tropical lower stratosphere, *J. Geophys. Res.*, *103*, 8651-8666, 1998.
- Neu, J.L., and R.A. Plumb, Age of air in a "leaky pipe" model of stratospheric transport, *J. Geophys. Res.*, *104*, 19,243-19,255, 1999.
- Newman, P.A., M.R. Schoeberl, R.A. Plumb, and J.E. Rosenfield, Mixing rates calculated from potential vorticity, *J. Geophys. Res.*, *93*, 5221-5240, 1988.
- Park, J. H., M. K. W. Ko, C. H. Jackman, R. A. Plumb, J. A. Kaye, and K. H. Sage, Editors, Models and Measurements Intercomparison II, *NASA Tech. Memo.*, *TM-1999-209554*, 1999.
- Plumb, R.A., A "tropical pipe" model of stratospheric transport, *J. Geophys. Res.*, *101*, 3957-3972, 1996.
- Prather, M.J., and E.E. Remsburg, The atmospheric effects of stratospheric aircraft: Report of the 1992 Models and Measurements Workshop, *NASA Ref. Publ.*, *1292*, vols. 1-3, 1993.
- Randel, W.J., and R.R. Garcia, Application of a planetary wave breaking parameterization to stratospheric circulation statistics, *J. Atmos. Sci.*, *51*, 1157-1168, 1994.
- Randel, W.J., F. Wu, J.M. Russell III, A. Roche, and J.W. Waters, Seasonal cycles and QBO variations in stratospheric CH<sub>4</sub> and H<sub>2</sub>O observed in UARS HALOE data, *J. Atmos. Sci.*, *55*, 163-185, 1998.
- Ray, E.A., F.L. Moore, J.W. Elkins, G.S. Dutton, D.W. Fahey, H. Vomel, S.J. Oltmans, and K.H. Rosenlof, Transport into the Northern Hemisphere lowermost stratosphere revealed by in situ tracer measurements, *J. Geophys. Res.*, *104*, 26,565-26,580, 1999.
- Rosenfield, J.E., D.B. Considine, P.E. Meade, J.T. Bacmeister, C.H. Jackman, and M.R. Schoeberl, Stratospheric effects of Mount Pinatubo aerosol studied with a coupled two-dimensional model, *J. Geophys. Res.*, *102*, 3649-3670, 1997.
- Sander, S.P., et al., Chemical kinetics and photochemical data for use in stratospheric modeling, Supplement to Evaluation 12: Update of key reactions, Evaluation number 13, *JPL Publ.*, *00-3*, 74 pp., 2000.
- Schoeberl, M.R., A.E. Roche, J.M. Russell III, D. Ortland, P.B. Hays, and J.W. Waters, An estimation of the dynamical isolation of the tropical lower stratosphere using UARS wind and trace gas observations of the quasi-biennial oscillation, *Geophys. Res. Lett.*, *24*, 53-56, 1997.
- Shia, R.-L., M.K.W. Ko, D.K. Weisenstein, C. Scott, and J.M. Rodriguez, Transport between the tropical and mid-latitude lower stratosphere: Implications for ozone response to high-speed civil transport emissions, *J. Geophys. Res.*, *103*, 25,435-25,446, 1998.
- Stolarski, R.S., et al., Scientific assessment of the atmospheric effects of stratospheric aircraft, *NASA Ref. Publ.*, *1381*, 110 pp., 1995.
- Strahan, S.E., A.R. Douglass, J.E. Nielsen, and K.A. Boering, The CO<sub>2</sub> seasonal cycle as a tracer of transport, *J. Geophys. Res.*, *103*, 13,729-13,741, 1998.
- Swinbank, R., and A. O'Neill, A stratosphere-troposphere assimilation system, *Mon. Weather Rev.*, *122*, 686-702, 1994.
- Volk, C.M., et al., Quantifying transport between the tropical and mid-latitude lower stratosphere, *Science*, *272*, 1763-1768, 1996.
- Volk, C.M., J.W. Elkins, D.W. Fahey, G.S. Dutton, J.M. Gilligan, M. Loewenstein, J.R. Podolske, K.R. Chan, and M.R. Gunson, Evaluation of source gas lifetimes from stratospheric observations, *J. Geophys. Res.*, *102*, 25,543-25,564, 1997.
- Waugh, D.W., et al., Mixing of polar vortex air into middle latitudes as revealed by tracer-tracer scatterplots, *J. Geophys. Res.*, *102*, 13,119-13,134, 1997.
- Weisenstein, D.W., M.K.W. Ko, J.M. Rodriguez, and

- N.D. Sze, Impact of heterogeneous chemistry on model-calculated ozone change due to HSCT aircraft, *Geophys. Res. Lett.*, *18*, 1991-1994, 1991
- Weisenstein, D.W., M.K.W. Ko, N.D. Sze, and J.M. Rodriguez, Potential impact of SO<sub>2</sub> emissions from stratospheric aircraft on ozone, *Geophys. Res. Lett.*, *23*, 161-164, 1996.
- World Meteorological Organization (WMO), Scientific Assessment of Ozone Depletion: 1998, *Rep. 44*, Global Ozone Res. and Monit. Proj., Geneva, 1999.

---

D. B. Considine, E. L. Fleming, C. H. Jackman, and R. S. Stolarski, NASA Goddard Space Flight Center, Code 916, Greenbelt Road, Greenbelt, MD 20771-0001. (fleming@kahuna.gsfc.nasa.gov)

(Received May 22, 2000; revised November 1, 2000, accepted November 7, 2000.)